Journal of Magnetism and Magnetic Materials 551 (2022) 169042

Contents lists available at ScienceDirect

Journal of Magnetism and Magnetic Materials

journal homepage: www.elsevier.com/locate/jmmm

Research articles

Polaronic corrections on magnetization and thermodynamic properties of electron–electron in 2D systems with Rashba spin–orbit coupling

K. Lakaal [a], M. Kria [a], J. El Hamdaoui [a], Varsha [b,c], V. Prasad [d], Vijit V. Nautiyal [b], M. El-Yadri [a], L.M. Pérez [e,*], D. Laroze [f], E. Feddi [a,**]

[a] Group of Optoelectronic of Semiconductors and Nanomaterials, ENSAM, Mohammed V University in Rabat, Rabat 10100, Morocco
[b] Department of Physics and Astrophysics, University of Delhi, Delhi 110007, India
[c] Department of Physics, Kalindi College, University of Delhi, Delhi 110008, India
[d] Department of Physics, Swami Shraddhanand College, University of Delhi, Delhi 110036, India
[e] Departamento de Física, FACI, Universidad de Tarapacá, Casilla 7 D, Arica 1000000, Chile
[f] Instituto de Alta Investigación, CEDENNA, Universidad de Tarapacá, Casilla 7 D, Arica 1000000, Chile

ARTICLE INFO

Keywords:
Rashba spin–orbit interaction
Electron–phonon coupling
Susceptibility
Heat capacity
Entropy
Quantum dots

ABSTRACT

Magnetic and thermodynamic properties of two electron system confined in 2-D quantum structures submitted to an applied magnetic field are studied taking into account the spin–orbit and electron–phonon interactions. The confinement is considered as a harmonic potential and the electron–electron interaction is taken as coulombic. We have first solved the Schrödinger equation to obtain energy levels and then obtain all the thermodynamic functions using canonical ensemble. The numerical calculation of our formalism is applied essentially for the GaN and InAs which are (III–V) compounds. Our results show that even at $B = 0$ T, the susceptibility of GaN shows diamagnetic behavior for all temperatures. However, with an increase in the magnetic field, susceptibility increases and the system shows paramagnetic behavior for both cases associated with and without polaron effect. We demonstrate that taking into account the Rashba spin–orbit interaction leads to a shift of the cutoff magnetic field Bc (value of B for which the magnetic nature of the dot changes from diamagnetic to paramagnetic) to the higher magnetic field with an increase in temperature. We also show that by taking into account the polaronic effect, Rashba spin–orbit interaction lowers the mean energy of the system. The heat capacity curve shows a peak at a low temperature (Schottky anomaly) and shifts toward high temperature with an increase in confinement and magnetic field strength. The consideration of the polaron effect shifts the heat capacity curve to lower temperatures.

1. Introduction

Recently, the progress and the mastery of the phenomena related to the spin and its interaction with the electronic system motion will certainly open the way to new applications in the spintronic area. Nowadays, spin-based nanodevices for optoelectronic applications and quantum transport constitute a challenging area for many researchers [1]. Based on the spin character instead of the charge carriers (electron and hole), this emerging field of spintronic devices use as a principle the interaction of the spin motion with the carrier orbits in semiconductor nanomaterials known as spin–orbit interaction (SOI) [2–5]. This concept is really impressive in confined systems and leads to more possibilities to discover other extraordinary non-conventional properties both in optoelectronic and in transport phenomena such as Qbit for memory and computing, coding the information, spin field-effect transistors, spin switch, spin LED, spin batteries, and many others devices [6].

Strictly speaking, the concept of spin–orbit interaction (SOI) can be considered as the result of the collective behavior of charge carriers and spin in asymmetrical systems. This coupling can occur through two situations: The first one corresponds to the Dresselhaus SOI (DSOI) induced in the case of bulk inversion asymmetry which corresponds to non-centrosymmetric crystal growth as in III–V and II–VI Zinc Blend and Wurtzite crystal structures [7]. The second situation is known as Rashba SOI (RSOI) takes place only in low dimensional structures and is caused by the asymmetry during the growth process especially in the heterostructure or by an external perturbation [8]. These two effects cause important changes in the optoelectronic, thermodynamic and

* Corresponding author.
** Corresponding author.
E-mail addresses: lperez@uta.cl (L.M. Pérez), e.feddi@um5s.net.ma (E. Feddi).

https://doi.org/10.1016/j.jmmm.2022.169042
Received 5 November 2021; Received in revised form 19 December 2021; Accepted 7 January 2022
Available online 5 February 2022

magnetic properties of nanomaterials. They are also very sensitive to the changes of the symmetry induced by the polar character of the materials (polaronic effects) or by external perturbations such as strain, temperature, magnetic and electric fields.

In the last decade, RSOI and DSOI have been extensively investigated in confined systems with different shapes and under different external perturbations. Interesting published works show the importance of the SOI on optoelectronic properties. Gisi et al. [9] have studied the effect of SOI on the optical properties of quantum wire submitted to a magnetic field. Their numerical results reveal that the optical properties of the nanowire are very sensitive to the SOI. Vaseghi and Ghaffari [10] have investigated this effect on the electronic structure of a monolayer quantum wire submitted to an electric field and magnetic field. They have demonstrated that the SOI has a different effect on the energy spectra according to the direction of the polarization of the electric field. Nautiyal et al. [11,12] have studied the effect of RSOI and DSOI on the second harmonic generation coefficients in the 2D quantum dot. The authors have also investigated the effect of a laser field and an external magnetic field on the multiphoton excitation in 2D quantum dot using the Kratzer potential. They have demonstrated that the current density of the system strongly depends on the laser parameters and the spin–orbit interaction. Recently, Rani et al. [13] have reported the energy levels of the 2 electrons system in 2D structures in presence of the magnetic field. In this model, the confinement is described by a potential having the following form: $V(r) = \alpha r^2 + \beta r + \frac{\gamma}{r} + \frac{\delta}{r^2}$ where $\alpha,\ \beta,\ \gamma\ and\ \delta$ are constants. However, the simultaneous effects of RSOI, DSOI, magnetic and electric fields on the nonlinear optical responses have been investigated in quantum rings of different shapes and sizes [14,15]. The authors point out that the resonant peaks shift to higher energy with increasing the eccentricity of the ring due to the SOIs. The effect of RSOI on the optical properties of quantum structures, such as quantum disk, coaxial quantum wire, and spherical quantum dot are also reported in the literature [16–19]. All these studies reveal that very important changes in the linear and the nonlinear optical properties of quantum heterostructures occur due to the SOI. Effects of RSOI and DSOI on the magnetization and thermodynamic properties of confined systems are also treated by several authors. Thus, the thermodynamic properties of nanowire submitted to a magnetic field taking into account the SOI has been treated in nanowire using a parabolic confinement [20]. The authors demonstrated that the specific heat and magnetic susceptibility admit peaks at low temperatures.

Generally, to understand the collective behavior of electrons, it is very convenient to treat the problem of two interacting electrons. The system of two electrons is considered one of the most attractive quantum systems. The investigation of the properties of few-electrons in quantum dots usually called as the artificial atoms have been extensively investigated both experimentally [21–24] and theoretically [25–28]. The exchange–correlation in such a quantum system allows a better comprehension of the behavior of the electronic system inside the confined systems. It has been demonstrated that the $electron-$ $-electron$ interactions play an important role in different physical properties of confined systems, for more details we refer the reader to the Refs. [29–36]. It is wroth mentioning that the effect of SOI and electron–electron interaction on the magnetic properties of materials have been analyzed by Kumar et al. [37], the authors have determined the magnetic properties of InAs QDs using canonical distribution. They have shown that the electron–electron interaction reduces the intensity of the magnetic properties. Their results show that RSOI causes a shift of the paramagnetic peak to higher magnetic field strength whereas the DSOI shifts it to the lower magnetic field region. They have remarked that the magnetization and susceptibility are independent on the SOI at larger temperatures. Khordad and Vaseghi [38,39] have studied the effect of the magnetic properties of InAs QD taking into account the RSOI by considering the interaction between 2 and 3 electrons. In both cases, the authors demonstrated the existence of a transition from diamagnetic to paramagnetism at low temperature and low magnetic field strength, they have remarked that the maximum of the susceptibility depends on both the interaction between the based electrons and SOI.

We recall that the Nitride-quantum dots and their heterostructures became a hot topic of research during the last two decades. They were used for violet–blue light sources and their large direct bandgap is used for LED and solar cell [40,41]. Even though these materials have been now regularly used to develop new optoelectronic devices, in the intersubband region, is yet to be fully explained as far as the development of new devices is concerned. Strictly speaking in such materials as GaN and InAs, the polaronic effect can influence the optoelectronic and thermal properties. It is well known that electron–phonon interactions depend strongly on the polarity of the materials. In addition, the polar character induces phonon of characteristics frequencies which are the hallmark of material. Although, these interactions are weaker compared to electron–electron Coulombic interactions but are comparable to spin–orbit interactions. There have been few works where the electronic properties of QDs in presence of electron–phonon interactions are studied. Huangfu and Yan [42] studied the effect of magnetic field on the binding energy of hydrogenic impurity taking into account electron–phonon interactions. Melnikov and Fowler [43] also studied the effect of electron–phonon interaction on the electronic properties of a spherical QD in a non-polar matrix [44]. Feddi et al. [45–47] have studied the influence of the electron–phonon and impurity ions in spherical quantum dots under magnetic and electric fields. In these studies, the authors have used the Fröhlich formalism [48] and Landau–Pekar transformation [49]. Their results show that the binding energy, diamagnetic response and polarizability are very sensitive to the polaronic effect [48].

The aim of this study is to show that taking into account the $electron$-phonon coupling in 2-D structures is unavoidable. This coupling is not only important from the basic physics point of view but also to show the lattice vibrations are crucial even if at low temperatures. In this paper we focus on the effect of electron–phonon coupling and RSOI on various magnetic and thermodynamic properties. Thus, we analyze the detailed study on thermodynamic and magnetic properties of 2D two electron Nitride-quantum structures taking into account the electron–electron interaction coupled via a Coulombic potential along with RSOI and the electron–phonon coupling. This paper is organized as follows: in Section 2, we describe the details of the theoretical model performed in the framework of the effective mass approximation and using the Fröhlichs approach for the polaronic part. Energy levels of the ground and the excited states are determined numerically and then used to obtain all thermodynamic and magnetic properties by considering the canonical ensemble approach. The numerical results and discussion are provided in Section 3. Finally, conclusions are drawn.

2. Model and theory

We start by outlining our theoretical approach in the determination of the thermal properties of GaN in bi-dimensional system material taking into account the electron–electron interactions. In the framework of the Boltzmann–Gibbs statistics, the thermodynamic and the magnetic properties will be investigated using the canonical partition function, $Z_c = \sum_i exp\left(-\beta E_i^{ee}\right)$, $\beta = 1/k_B T$ and k_B is the Boltzmann constant. T is the temperature expressed in Kelvin. We note that the summation relates to all the energies levels E_i^{ee} of the system obtained by solving the Schrödinger equation $\mathcal{H}_{ee}|i\rangle = E_i^{ee}|i\rangle$. In this approach, the main thermodynamic properties of the system can be deduced using Z_c: The mean energy of the system is calculated using the expression:

$$\langle E\rangle = k_B T^2 \frac{\partial \ln Z_c}{\partial T}, \tag{1}$$

the heat capacity defining the quality of energy storage:

$$C_v = -k_B \beta^2 \left(\frac{\partial \langle E\rangle}{\partial \beta}\right) \tag{2}$$

and finally, the entropy, which is considered among the most important thermodynamic properties; it describes the randomness of the system. It can be obtained through the relation:

$$S = k_B \beta(\langle E\rangle - F_H), \tag{3}$$

where $F_H = F = -k_B T \ln Z_c$ is the Helmholtz free energy describing the stability criterion. We also recall that the determination of the degree of magnetization of a given material submitted to a magnetic field (B) can be determined by the magnetic susceptibility ($\chi = \frac{\partial M}{\partial B}$). It indicates the paramagnetism ($\chi > 0$) or diamagnetism ($\chi < 0$) characters of the material. The magnetization M can be extracted from the statistical relation:

$$M = \frac{-1}{Z_c}\sum_i \frac{\partial E_i^{ee}}{\partial B} exp\left(-\beta E_i^{ee}\right). \tag{4}$$

From the above, we understand that the determination of the energy spectrum of the system is a must. As first step, let us focus on the energy spectrum of two interacting electrons confined in 2D materials submitted to a perpendicular magnetic field $\vec{B} = (0,0,B)$ which is described in the Lorentz gauge by the vector potential $\vec{A} = \frac{1}{2}(\vec{B}\times\vec{r})$. By taking into consideration the interaction with LO-phonon and RSOI effects, the energy of the system is solution of the equation $\mathcal{H}_{ee}|i\rangle = E_i^{ee}|i\rangle$ where $\mathcal{H}_{ee}$ is the Hamiltonian expressed in the xy plane as:

$$\mathcal{H}_{ee} = \mathcal{H}_0 + V_c + \mathcal{H}_R^{SO} + \mathcal{H}_z + \mathcal{H}_{ph} + \mathcal{H}_{e-ph} \tag{5}$$

In Eq. (5) H_0 is the Hamiltonian of confined interacting electrons defined as

$$\mathcal{H}_0 = \frac{1}{2m_e^*}\sum_{i=1}^{2}\left(\vec{P}_i + \frac{e\vec{A}_i}{c}\right)^2 + \sum_{i=1}^{2} V_w\left(r_i\right) \tag{6}$$

where m_e^* is the effective mass of the electron, e is the electron charge and $\vec{P_i}$ is the momentum of the electron i. In this study we suppose that the confinement will be described by a parabolic potential, $V_w\left(r_i\right)$ given by

$$\sum_{i=1}^{2} V_w\left(r_i\right) = \frac{1}{2}m_e^*\omega_0^2\sum_{i=1}^{2} r_i^2 \tag{7}$$

where $\hbar\omega_0$ is the confinement strength. The coulombic potential is given by $V_c = \frac{e^2}{\epsilon_\infty|\vec{r}_1-\vec{r}_2|}$, where ϵ_∞ is the high-frequency dielectric constant. The third term $\mathcal{H}_R^{SO}$ denotes the Rashba spin–orbit Hamiltonian expressed as follows [38]:

$$\begin{aligned}\mathcal{H}_R^{SO} &= \frac{\alpha_R}{\hbar}\sum_{i=1}^{2}\left[\hat{\sigma}_i \times \left(\hat{P}_i + \frac{e\hat{A}_i}{c}\right)\right] \\ &= \frac{\alpha_R}{\hbar}\sum_{i=1}^{2}\left[\hat{\sigma}_{x,i}(\hat{P}_{y,i} + \frac{e\hat{A}_{y,i}}{c}) - \hat{\sigma}_{y,i}(\hat{P}_{x,i} + \frac{e\hat{A}_{x,i}}{c})\right]\end{aligned} \tag{8}$$

α_R is the Rashba coupling constant, c is the speed of electromagnetic waves in vacuum and σ_x, σ_y and σ_z are the Pauli matrices. The fourth term in Eq. (5) is the Zeeman term:

$$\mathcal{H}_Z = \frac{1}{2}g^*\mu_B B\sum_{i=1}^{2}\sigma_{z,i} \tag{9}$$

g^* is the Lande's factor of the electron and $\mu_B = \frac{e\hbar}{2m_0c}$ is the Bohr magneton. Using the Fröhlich's continuum formalism [45], the last two terms in Eq. (5) describe the kinetic operator of phonon

$$\mathcal{H}_{ph} = \sum_{\vec{q}} \hbar\omega_{LO}\hat{a}_{\vec{q}}^+\hat{a}_{\vec{q}} \tag{10}$$

where $\hat{a}_{\vec{q}}^+(\hat{a}_{\vec{q}})$ is the creation (destruction) operator of the phonon with wave vector $\vec{q}$ and the Hamiltonian representing the *electron*-phonon coupling:

$$\mathcal{H}_{e-ph} = \sum_{\vec{q}}\left[\hat{a}_{\vec{q}}V_{\vec{q}}(\exp(i\vec{q}\vec{r_1}) + \exp(i\vec{q}\vec{r_2})) + h.c\right] \tag{11}$$

where the coefficient of electron–phonon coupling is given by

$$V_{\vec{q}} = \left[\frac{2\pi e^2}{V}\frac{\hbar\omega_{LO}}{q^2}\left(\frac{1}{\epsilon_\infty} - \frac{1}{\epsilon_0}\right)\right]^{1/2} \tag{12}$$

where V is the volume of the crystal and ϵ_0 is the static dielectric constant.

In order to solve the Schrödinger equation $\mathcal{H}_{ee}|i\rangle = E_i^{ee}|i\rangle$, firstly, we introduce the relative and the center of mass (CM) parameters: ($\vec{r} = \vec{r_1} - \vec{r_2}$ and $\vec{R} = \frac{\vec{r_1}+\vec{r_2}}{2}$ for coordinates, $\mu = m_e^*/2$ and $M_0 = 2m_e^*$ for masses). By considering the Lee Low Pines (LLP) transformation [48] the polaronic contribution can be simplified and the total expression of the Hamiltonian given by the (Eq. (5)) takes the following form:

$$\begin{aligned}\mathcal{H}_{ee} &= \frac{P_r^2}{2\mu} + \frac{e^2}{\epsilon_\infty r} + \frac{1}{2}\mu\Omega^2 r^2 + \frac{1}{2}\omega_c L_z \\ &+\alpha_{LO}\hbar\omega_{LO} - \frac{2\alpha_{LO}\hbar\omega_{LO}}{u_{LO}r}(1-\exp(-u_{LO}r)) - \alpha_{LO}\hbar\omega_{LO}\exp(-u_{LO}r) \\ &+\frac{P_R^2}{2M_0} + \frac{1}{2}M_0\Omega^2R^2 + \frac{1}{2}\omega_c L_Z + \frac{\alpha_R}{\hbar}\begin{pmatrix} 0 & H_{12} \\ H_{21} & 0\end{pmatrix} \\ &+g^*\mu_B B\begin{pmatrix} 1 & 0 \\ 0 & -1\end{pmatrix}\end{aligned} \tag{13}$$

Where $\Omega^2 = \frac{\omega_c^2}{4} + \omega_0^2$, $\omega_c = \frac{eB}{m^*c}$. $L_z = m\hbar$ and $L_Z = M\hbar$ are the z-component of angular momentum in relative and CM part respectively, m and M are the angular momentum quantum numbers of relative part and CM respectively. Both m and M can take the values $0, \pm1, \pm2....$ The size $\frac{1}{u_{LO}}$ of the two interacting electrons and the *electron*-phonon coupling constant α_{LO} are defined, respectively, as

$$u_{LO} = \sqrt{\frac{2M_0\omega_{LO}}{\hbar}}, \alpha_{LO} = \frac{e^2}{2\hbar\omega_{LO}}\left(\frac{2M_0\omega_{LO}}{\hbar}\right)^{1/2}\left(\frac{1}{\epsilon_\infty} - \frac{1}{\epsilon_0}\right). \tag{14}$$

As we can see, the Hamiltonian (Eq. (13)) is a sum of two independent parts: $\mathcal{H}_{ee} = \mathcal{H}_{rel} + \mathcal{H}_{CM}$ and consequently the energy spectrum of the system is $E^{ee} = E_{CM} + E_{rel}$. Therefore We can write:

$$\mathcal{H}_{rel} = \mathcal{H}_{rel}^0 + V_{e-ph}^{int} \tag{15}$$

where

$$\mathcal{H}_{rel}^0 = \frac{P_r^2}{2\mu} + \frac{1}{2}\mu\Omega^2 r^2 + \frac{1}{2}\omega_c L_z \tag{16}$$

and

$$V_{e-ph}^{int} = \frac{e^2}{\epsilon_\infty r} - \frac{2\alpha_{LO}\hbar\omega_{LO}}{u_{LO}r}(1-\exp(-u_{LO}r)) - \alpha_{LO}\hbar\omega_{LO}\exp(-u_{LO}r) \tag{17}$$

According to this approach, the wave function $\psi_{n,m}(r,\phi)$ corresponding to relative motion given by:

$$\psi_{n,m}(r,\phi) = \exp(im\phi)f_{n,m}(r) \tag{18}$$

Where

$$f_{n,m}(r) = \left(\frac{2a^2 n!}{(n+|m|)!}\right)^{1/2}(ar)^{|m|}L_n^{|m|}(a^2r^2)\exp(-a^2r^2/2) \tag{19}$$

in which $a = \sqrt{\frac{\mu\Omega}{\hbar}}$ is the inverse of the effective dot size, which indicates both the degree of confinement caused by the size and the magnetic field effects. $L_n^{|m|}(a^2r^2)$ is the Laguerre polynomial.

In the relative donor units $a^* = \frac{\epsilon_0\hbar^2}{\mu e^2}$ for length and $R^* = \frac{\hbar^2}{2\mu a^{*2}}$ for the energy the energies without polaronic term, E_{rel}^0 can be determined exactly by solving: $\mathcal{H}_{rel}^0 f_{n,m}(r) = E_{rel}^0 f_{n,m}(r)$. It written as:

$$E_{rel}^0 = 2\gamma_1(2n + |m| + 1) + m\gamma_2 \tag{20}$$

where $\gamma_1 = \frac{\hbar\Omega}{2R^*}$ and $\gamma_2 = \frac{\hbar\omega_c}{2R^*}$. n and m are the radial quantum number and the angular momentum quantum number respectively.

By considering the *electron*-phonon coupling, the relative energy can be determined by computing the complete energy expression:

$$E_{rel} = 2\gamma_1(2n + |m| + 1) + m\gamma_2 + \left\langle f_{n,m}\left|V_{e-ph}^{int}(r)\right|f_{n',m'}\right\rangle \tag{21}$$

where the mean value of the *electron−electron* interaction and *electron*-phonon interaction is obtained by determining the matrix elements:

$$\left\langle \psi_{n,m}|V^{int}_{e-ph}(r)|\psi_{n',m'}\right\rangle = \int_0^\infty r f^*_{n,m}(r)V^{int}_{e-ph}(r)f_{n',m'}(r)\delta_{nn'}\delta_{mm'}dr \tag{22}$$

$\delta_{nn'}$ and $\delta_{mm'}$ are the Kronecker delta symbols.

On the other hand the CM Hamiltonian is presented by the following operators:

$$\mathcal{H}_{CM} = \frac{P_R^2}{2M_0} + \frac{1}{2}M_0\Omega^2R^2 + \frac{1}{2}\omega_c L_Z + \frac{\alpha_R}{\hbar}\begin{pmatrix} 0 & H_{12} \\ H_{21} & 0 \end{pmatrix} + g^*\mu_B B\begin{pmatrix} 1 & 0 \\ 0 & -1 \end{pmatrix} \tag{23}$$

Where $\mathcal{H}_{12}$ and $\mathcal{H}_{21}$ are the expressions obtained by the development of the matrix element of the Rashba operator term given as:

$$\begin{cases} \mathcal{H}_{12} = \hbar e^{-i\Phi}\left[\frac{\partial}{\partial R} - \frac{i}{R}\frac{\partial}{\partial \Phi} + \frac{eB}{c}R\right] \\ \mathcal{H}_{21} = \hbar e^{+i\Phi}\left[-\frac{\partial}{\partial R} - \frac{i}{R}\frac{\partial}{\partial \Phi} + \frac{eB}{c}R\right] \end{cases} \tag{24}$$

By considering a wave function as the product of independent angular and radial terms:

$$\Psi_{N,M}(R,\Phi) = \begin{cases} U_N(R)e^{iM\Phi} \\ V_N(R)e^{i(M+1)\Phi} \end{cases} \tag{25}$$

N and M are the principal and magnetic quantum numbers of CM states.

Under these conditions the Hamiltonian takes the form:

$$\mathcal{H}_{CM} = \begin{cases} -\frac{1}{4}\left(\frac{\partial^2}{\partial R^2} + \frac{1}{R}\frac{\partial}{\partial R} + k^2 - \frac{M^2}{R^2}\right)U_N(R) + 4\gamma_1^2R^2U_N(R) \\ \quad +\alpha\left(\frac{\partial}{\partial R} + \frac{M+1}{R}\right)V_N(R) + 2\alpha\gamma_2 RV_N(R) = 0 \\ -\frac{1}{4}\left(\frac{\partial^2}{\partial R^2} + \frac{1}{R}\frac{\partial}{\partial R} + q^2 - \frac{(M+1)^2}{R^2}\right)V_N(R) + 4\gamma_1^2R^2V_N(R) \\ \quad +\alpha\left(-\frac{\partial}{\partial R} + \frac{M}{R}\right)U_N(R) + 2\alpha\gamma_2 RU_N(R) = 0 \end{cases} \tag{26}$$

where $k^2 = -M\gamma_2 - \frac{g^*\mu_B B}{R^*} + \epsilon_R$, $q^2 = -(M+1)\gamma_2 + \frac{g^*\mu_B B}{R^*} + \epsilon_R$, $\epsilon_R = \frac{E_{CM}}{R^*}$ and $\alpha = \frac{\alpha_R}{R^*a^*}$.

To solve Eqs. (26) we consider the following forms for the CM wave functions written linear combination of Bessel functions:

$$\begin{cases} U_N(R) = AJ_M(kR) + BJ_M(qR) \\ V_N(R) = AJ_{M+1}(kR) + BJ_{M+1}(qR) \end{cases} \tag{27}$$

In the following, we consider only the fundamental state of CM motion which corresponds to $N = 1$ and $M = 0$, Then, the energy eigen values E_{CM} can be determined by a numerical resolution of the differential equations $\mathcal{H}_{CM}\ \Psi_N(R,\Phi) = E_{CM}\Psi_N(R,\Phi)$.

3. Results and discussions

The numerical calculation of our formalism is applied essentially to the GaN is an (III–V) group compound. Contrary to the majority of the (III–V) semiconductors, GaN, has an important polar character with a coupling constant ($\alpha_{LO} = 0.439$) [50] which implies the existence of a strong interaction between charge carriers and phonon. In order to analyze the effect of *electron* -phonon coupling strength, we also apply our model for another (III–V) compound ($InAs$) characterized by weak *electron*-phonon coupling ($\alpha_{LO} = 0.055$) [51] which explains its weak polarity. We underline that for most (IIIV) compounds, the constant *electron*-phonon coupling is less than 1 which justifies Fröhlichs perturbation theory. All the physical parameters used in this study are listed in Table 1, extracted from the references cited in the same table. We used two length scales to characterize the relative strengths in the interplay of confinement and SO interaction: $l_0 = \sqrt{\frac{\hbar}{m_e^*\omega_0}}$, $l_s = \sqrt{\frac{\hbar^2}{2m_e^*\alpha_R}}$, where l_0 is the characteristic length corresponding to the confinement potential and l_s is the length associated with SO interaction.

In this work we focalize our self on two limit values of confinement strength: $l_0 = 5$ nm ($\hbar\omega_0 = 16.9$ meV) and $l_0 = 10$ nm($\hbar\omega_0 = 4.2$ meV). The first case corresponds to a strong confinement case with $l_0 \le a^*$ (a^* is the Bohr radius given in Table 1) while the second case corresponds to a weak confinement with $l_0 \succ a^*$.

We recall that the energy levels of the 2 electrons quantum dot in a magnetic field with RSOI and taking into account the *electron*-phonon coupling are obtained by the procedure mentioned in the model and theory section. As shown in the previous section the energy of the system of 2 electrons $E^{ee} = E_{CM} + E_{rel}$ contains both effects: The RSOI term comes into the E_{CM} expression while the *electron*-phonon coupling strength modifies E_{rel}. It is well known that due to α_R (RSOI coefficient) the degeneracy of the levels are lifted. Even without SOI, Zeeman splitting occurs, and the findings are not displayed here, but the splitting is comparable to those discovered in ref [11,12] and the level splitting is considerably more pronounced in our case.

It is well known that magnetic susceptibility is an important parameter that defines the degree of magnetization of the system. Also, it defines the nature of magnetic property as the diamagnetism or paramagnetism and it also allows to study that whether diamagnetic to paramagnetic conversion is possible in presence of the magnetic field, or if there are parameters that can control this transition.

In Fig. 1, we present the susceptibility (χ) of GaN QD as a function of magnetic field strength given by the ratio ω_c/ω_0 for a fixed parabolic confinement potential $\hbar\omega_0 = 4.2$ meV corresponding to $l_0 = 10$ nm and for three values of temperature ($T = 1, T = 50$ and $T = 100$ K). The dashed lines and solid lines represent the case without and with RSOI respectively ($\alpha_R = 0$ and $\alpha_R = 2\times10^{-11}$ (eV m)). It is interesting to note that even at $B = 0$ T, the QD shows diamagnetic behavior ($\chi \prec 0$) for all temperatures considered and for both cases of with and without *electron*-phonon interactions given in Fig. 1a and Fig. 1b respectively. However, for the case where *electron*-phonon interactions are neglected ($V_{e-ph} = 0$), the susceptibility is more pronounced than the case where this interaction is non-zero ($V_{e-ph} \ne 0$). In both cases ($V_{e-ph} = 0$ and $V_{e-ph} \ne 0$), we can remark that with an increase in the magnetic field, susceptibility increases and the system shows paramagnetic behavior ($\chi \succ 0$) at the moderate magnetic field ($\omega_c/\omega_0 = 4$ or $B \simeq 26$ T) when RSOI is neglected and at ($\omega_c/\omega_0 = 7$ or $B \simeq 46$ T) when RSOI is taken into consideration. Indeed, we can remark that at high magnetic field, the susceptibility presents a diamagnetic character when the RSOI is not taken into account ($\alpha_R = 0$). Surprisingly this behavior change absolutely in the case when the RSOI is not neglected ($\alpha_R \ne 0$), and the paramagnetic character of the material persists. So the susceptibility tends to a saturation positive value. In contrast to the case, $V_{e-ph} = 0$, $V_{e-ph} \ne 0$ case presented in Fig. 1b shows a remarkable behavior: after a maximum, the susceptibility decreases very slowly and tends to a saturation regime. The GaN QD shows a paramagnetic character even at larger magnetic field values. This is quite interesting, showing that the magnetic nature of GaN QD can be manipulated much strongly with *electron*-phonon coupling strength. However, with the introduction of spin–orbit interaction, the cutoff magnetic field B_c (where the magnetic nature of the dot changes over from diamagnetic to paramagnetic) shifts to the higher magnetic field ($\frac{\omega_c}{\omega_0} \simeq 7$ or $B \simeq 46$ T). We note that in the case when the RSOI ($\alpha_R \ne 0$) and without taking into account the *electron*-phonon coupling the susceptibility shows two peaks, the first is located at weak magnetic field ($\frac{\omega_c}{\omega_0} \simeq 3$) and the second is observed at high magnetic field ($\frac{\omega_c}{\omega_0} \simeq 8.5$). These two peaks give approximatively the values of the ratio ω_c/ω_0 for which the both phases diamagnetic and paramagnetic are maximum. This phenomenon disappears when the electron–phonon coupling is not neglected as shown in Fig. 1b.

The magnetization parameter M is given by Eq. (4) is the ability of the sample to retain induced magnetism in the presence of the magnetic field. The results are presented for $\alpha_R \ne 0$ and $\alpha_R = 2\times10^{-11}$ (eV m) and also with taking into account the electron–phonon coupling.

Table 1
GaN and $InAs$ material parameters used in the calculations extracted from [50,52–55] for GaN and [51,56–58] for $InAs$.

$Material$	$\frac{m_e^*}{m_0}$	$\frac{m_h^*}{m_0}$	E_g (eV)	ϵ_0	ϵ_∞	a^* (nm)	R^* (meV)	$\hbar\omega_{LO}$ (meV)	$\hbar\omega_{TO}$ (meV)	α_{LO}	α_R (10^{-11} meV × m)
GaN	0.20	1.25	3.39	9.5	5.35	5.59	13.56	91.2	69.43	0.439	2
InAs	0.023	0.33	0.42	15.2	12.3	70	0.68	19	30.1	0.055	(1-5)

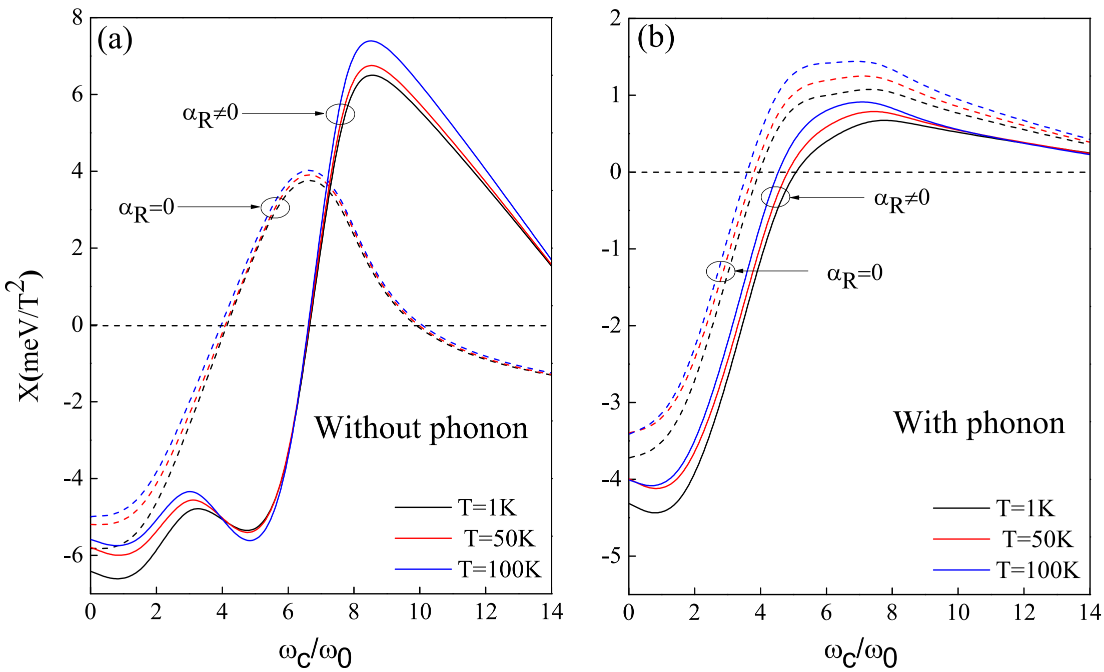

Fig. 1. Plot of susceptibility of GaN QD as function of ω_c/ω_0 (l_0 = 10 nm and $\hbar\omega_0$ = 4.2 meV) for three values of temperature T = 1 K, T = 50 K and T = 100 K. The dashed lines and solid lines represent the case without and with RSOI respectively (α_R = 0 and $\alpha_R \neq 0$).

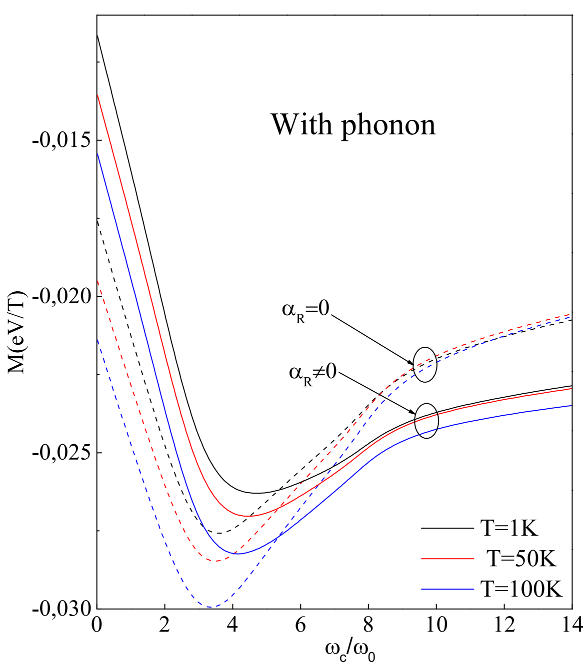

Fig. 2. Plot of Magnetization for GaN vs ω_c/ω_0 for three values of temperature T = 1 K, T = 50 K and T = 100 K with $\hbar\omega_0$ = 4.2 meV. The dashed lines and solid lines are represent the case without and with RSOI respectively (α_R = 0 and $\alpha_R \neq 0$).

Fig. 2 displays the variation of the magnetization $\chi = \frac{dM}{dB}$ as a function of the frequency ratio $\frac{\omega_c}{\omega_0}$ taking into account the phonon effects. In addition, in order to analyze the effect of SOI, we have presented the two cases with and without the RSOI. As we can see, we can distinguish 2 principal regions: In the first region, $\frac{\omega_c}{\omega_0} \lesssim 4$ or $B \lesssim 26$ T we can see that for a given B the RSOI reinforces the magnetization of the system. However, This situation is inversed in the second region $\frac{\omega_c}{\omega_0} \gtrsim 7$ or $B \gtrsim 46$ T, the RSOI reduces the Magnetization. An important remark to highlight: looking at the general behavior of the magnetization with or without RSOI shows that the parameter M decreases towards a minimum then changes its variation and begins to increase up to a limit value presenting saturation. The minimums tend to move towards the weak intensities of the magnetic field as the temperature increases. According to the definition, the susceptibility describes the slope of the magnetization $\chi = \frac{dM}{dB}$ in the diagram (M, B), thus, as shown in Fig. 2, before the minimum the magnetization decreases ($\frac{dM}{dB} \prec 0$) which means that material has a diamagnetic character ($\chi \prec 0$), After this minimum, the magnetization increases and admits a positive slope ($\frac{dM}{dB} \succ 0$) which explains the paramagnetic character of the system ($\chi \succ 0$).

The analysis of mean energy is important since it affects the partition function, and thus we can measure the thermodynamic properties of the system by understanding the behavior of energy and partition function. Fig. 3a shows the variation of mean energy for GaN against the temperature for two confinement strengths $\hbar\omega_0$ = 4.2 meV and $\hbar\omega_0$ = 16.9 meV and for B = 20 T and α_R = 2×10^{-11} (eV m). The dashed lines and solid lines are associated without and with the polaron effect, respectively. We observe that with an increase in temperature, the mean energy of the system also increases. This is because as temperature increases, the kinetic energy of the system becomes more important. By reinforcing the confinement strength (from $\hbar\omega_0$ = 4.2 meV to $\hbar\omega_0$ = 16.9 meV), the mean energy increases. Our calculations show an important result it allows us to confirm that the

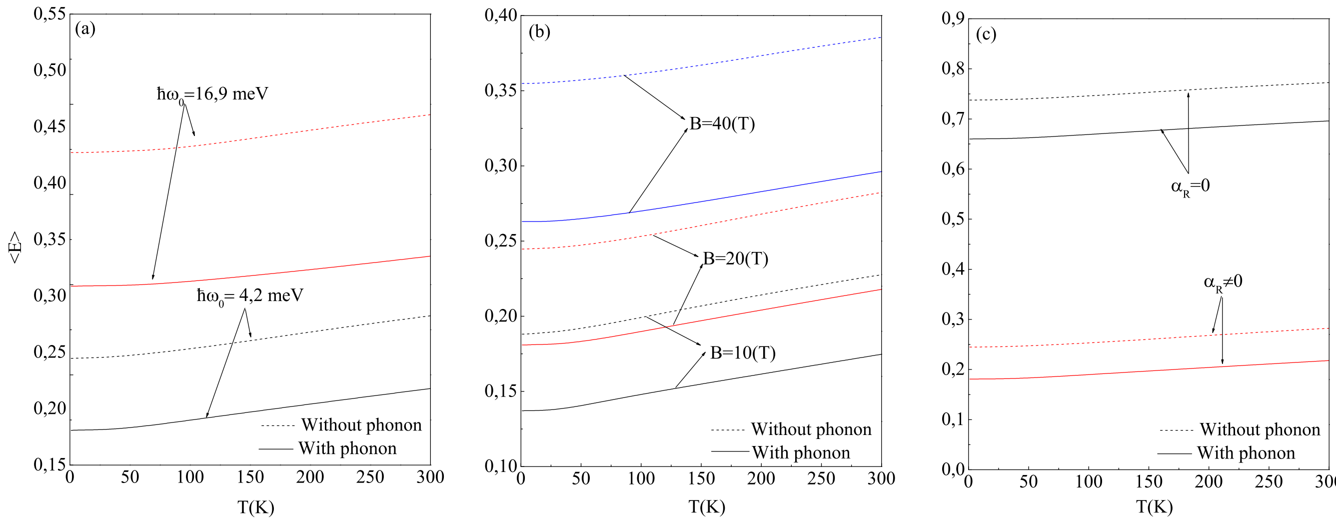

Fig. 3. Plot of mean energy for GaN vs temperature, (a) for two values of confinement strength $\hbar\omega_0 =$ 4.2 meV *and* $\hbar\omega_0 =$ 16.9 meV at $B = 20$ T and $\alpha_R = 2\times10^{-11}$ (eV m). (b) for three values of magnetic field strength $B = 10, B = 20$ and $B = 40$ T , with $\hbar\omega_0 =$ 4.2 meV, and $\alpha_R = 2\times10^{-11}$ (eV m). (c) without and with RSOI at $B = 20$ T and $\hbar\omega_0 =$ 4.2 meV. The dashed lines and solid lines are associated without and with polaron effect, respectively in all figures.

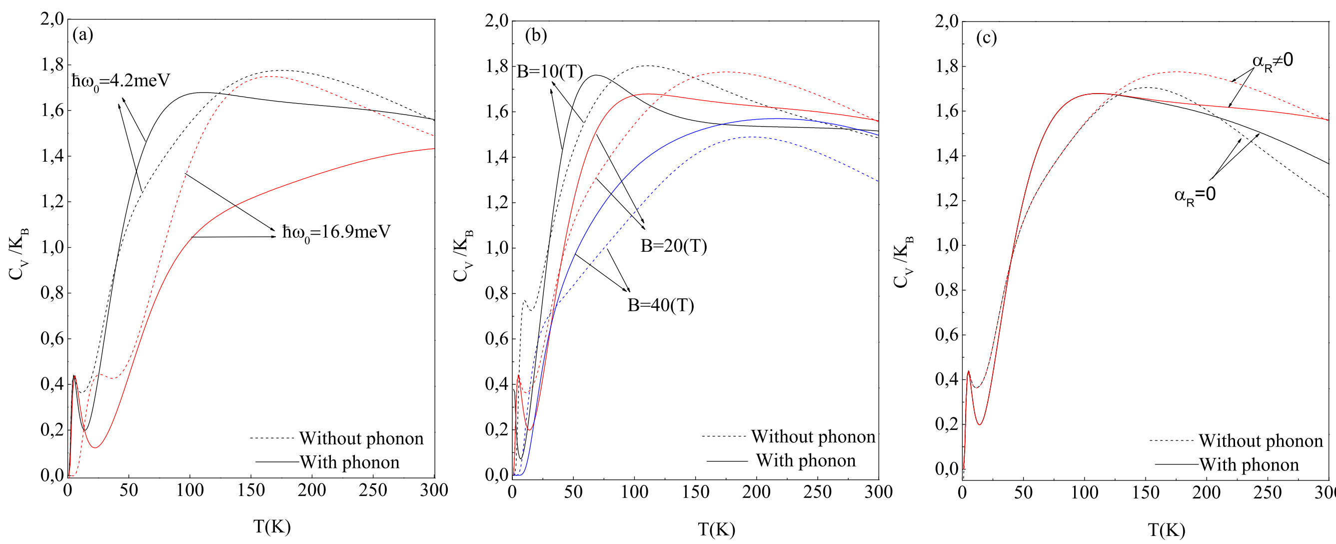

Fig. 4. Plot of heat capacity for GaN vs temperature, (a) for two values of confinement strength $\hbar\omega_0 =$ 4.2 meV *and* $\hbar\omega_0 =$ 16.9 meV at $B = 20$ T and $\alpha_R = 2\times10^{-11}$ (eV m). (b) for three values of magnetic field strength $B = 10, B = 20$ and $B = 40$ T, with $\hbar\omega_0 =$ 4.2 meV, and $\alpha_R = 2\times10^{-11}$ (eV m). (c) without and with RSOI at $B = 20$ T and $\hbar\omega_0 =$ 4.2 meV. The dashed lines and solid lines are associated without and with polaron effect, respectively in all figures.

phonon interactions reduce the total energy of the system, it is clear the polaron affects considerably the mean energy.

Fig. 3b displays the variation of mean energy for GaN vs temperature with magnetic field $B = 10, 20$ and 40 T and for $\alpha_R = 2\times10^{-11}$ (eV m) and $\hbar\omega_0 = 4.2$ meV. The dashed lines and solid lines are associated without and with the polaron effect, respectively. With an increase in the magnetic field strength, the mean energy of the system also increases. There is a decrease of approximately $0.05eV$ in mean energy value with consideration of the polaron effect. Similarly, to understand the behavior of mean energy with RSOI, we have obtained Fig. 3c, which shows the variation of mean energy for GaN vs temperature with and without RSOI. The dashed lines and solid lines are associated without and with the polaron effect, respectively for $B = 20$ T and $\hbar\omega_0 = 4.2$ meV. The presence of RSOI lowers the mean energy of the system by approximately 0.5 meV. Here too, the presence of polaron effect consideration lowers the mean energy by approximately 0.05 eV.

The heat capacity variation for GaN for two confinement strengths of $\hbar\omega_0 = 4.2$ meV and $\hbar\omega_0 = 16.9$ meV with temperature (in K) and $B = 20$ T and $\alpha_R = 2\times 10^{-11}$ (eV m) is shown in Fig. 4a, where the dashed lines and solid lines are associated without and with the polaron effect, respectively. We can remark that up to 20 K, the heat capacity with the polaron effect has the same behavior for both confinement strengths ($\hbar\omega_0 = 4.2$ meV and $\hbar\omega_0 = 16.9$ meV), however without polaron effect, with an increase in confinement strength (from $\hbar\omega_0 = 4.2$ meV to $\hbar\omega_0 = 16.9$ meV), for this low range of up to 20 K, the behavior of heat capacity on the two confinement strength are opposite to each other. From a temperature of 25 K onwards, the heat capacity for $\hbar\omega_0$=16.9meV increases with an increase in temperature and then tends to saturate toward 300 K. However, without the polaron effect with $\hbar\omega_0 = 4.2$ meV and $\hbar\omega_0 = 16.9$ meV, for about 150K, the heat capacity curve attains a maximum and then starts decreasing but for $\hbar\omega_0 = 4.2$ meV confinement strength with polaron effect, the peak appears around 80K. It is interesting to note that for 16.9 meV confinement strength without polaron effect heat capacity is larger compared to the with polaron effect whereas in 4.2meV confinement strength before 100K heat capacity with polaron effect is larger and after that without polaron effect heat capacity is dominant.

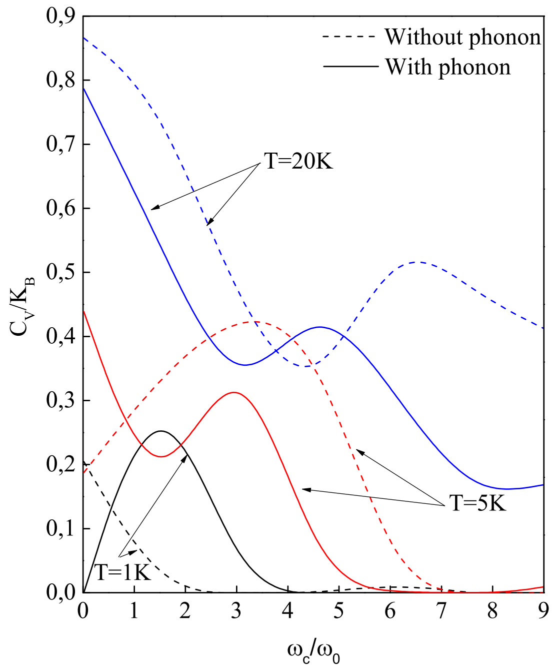

Fig. 5. Plot of heat capacity for GaN vs ω_c/ω_0 for three values of temperature T = 1 K, T = 5 K and T = 20 K, with $\hbar\omega_0$ = 4.2 meV and α_R = 0. The dashed lines and solid lines are associated without and with polaron effect, respectively.

Fig. 4b shows the variation of the heat capacity variation for GaN vs temperature for three different magnetic fields B = 10, 20 and 40 T for $\hbar\omega_0$ = 4.2 meV and $\alpha_R = 2\times 10^{-11}$ (eV m). The dashed lines and solid lines are associated without and with the polaron effect, respectively. We observe a peak in the heat capacity curve at a particularly low temperature and below and after that value of temperature, heat capacity decreases. The heat capacity curves shift toward high temperature with an increase in magnetic field strength with a decrease in the peak height. With the polaron effect heat capacity is dominant below 75 K for 10 T magnetic field, whereas for 20 T magnetic field strength, it is dominant below 125 K but for 40 T, above 50 K heat capacity with polaron effect is dominant.

The Rashba term affects the heat capacity for the temperature of above 100 K as shown in Fig. 4c. It shows the variation of the heat capacity variation for GaN with temperature with $\hbar\omega_0$ = 4.2 meV and B = 20 T for with and without Rashba term $\alpha_R = 2\times 10^{-11}$ (eV m). The dashed lines and solid lines are associated without and with the polaron effect, respectively. The consideration of the polaron effect shifts the heat capacity curve to lower temperatures. It is worth mentioning that the peaks obtained at low temperature correspond to Schottky anomaly [28,59,60].

For a better understanding of the confinement strength effect, we have obtained Fig. 5 which shows the variation of the heat capacity variation for GaN for different temperatures of 1 K,5 K and 20 K with ω_c/ω_0 for $\hbar\omega_0$ = 4.2 meV and $\alpha_R = 2\times 10^{-11}$ (eV m). The dashed lines and solid lines are associated without and with the polaron effect, respectively. As we increase the temperature, with an increase in ω_c/ω_0, we observe that the heat capacity with polaron effect at 1K shows a peak and then decreases to zero, at 5 K it decreases from a maximum value and then starts increasing from that point of ω_c/ω_0 where the maxima of 1 K heat capacity occurred and reach a maximum where heat capacity curve with polaron effect touches zero for 1 K temperature and then decreases to zero after that. Similarly, for 20 K, it first decreases from a maximum and then starts increasing from that point of ω_c/ω_0 where the maxima of 5 K heat capacity with polaron effect occurred and reach a maximum where the heat capacity curve touches zero for 5 K temperature and then decreases and saturates around 0.15. Without the polaron effect, heat capacity shows a similar kind of behavior but 20 K and 5 K, without taking into account polaron interaction the heat capacity is higher than when the polaron interaction concept is used whereas, for 1 K, heat capacity with the polaron effect is dominant then without polaron effect consideration.

Entropy explains the order and randomness in the system. Fig. 6a shows variation of entropy for GaN with temperature with confinement strengths $\hbar\omega_0$ = 4.2 meV and $\hbar\omega_0$ = 16.9 meV. The dashed lines and solid lines are associated without and with polaron effect, respectively with B = 20 T and $\alpha_R = 2\times 10^{-11}$ (eV m). The entropy of the system increases with an increase in temperature as it increases the randomness of the system by increasing the energy. With a decrease in confinement strength the entropy increases as the energy of the system increases. The polaron effect consideration increases the entropy in small confinement strength ($\hbar\omega_0$ = 4.2 meV) whereas with large confinement strength ($\hbar\omega_0$ = 16.9 meV), at low temperature(below 150 K) entropy is large than at high temperature (above 150 K).

With an increase in magnetic field strength, the entropy decreases, and the consideration of the polaron effect decrease it further as shown in Fig. 6b which shows entropy with temperature for different magnetic field strength at $\hbar\omega_0$=4.2meV and $\alpha_R = 2\times 10^{-11}$ (eV m). The solid lines are for curves with consideration of polaron effect and dotted lines are without polaron effect consideration.

Helmholtz's free energy tells us about the useful work done that is obtained from a system or we can define it as the energy required to create a system at constant temperature and volume, therefore it tells us the stability criterion. Fig. 7 shows the variation of Helmholtz's free energy of GaN as a function of temperature with polaron effect (solid lines) and without polaron effect (dashed lines). All curves presented in Fig. 7 show a decrease of Helmholtz's free energy with an increase in temperature, as increasing temperature causes the increase in entropy so Helmholtz's free energy decreases. Strictly speaking Fig. 7a displays this variation taking into account the RSOI. Our results show that the Helmholtz free energy is strongly dependent on the RSOI. The shift is very important and can reach about (0.5 eV) for both cases with and without phonon. Based on this important observation, it is recommended that the RSOI cannot be neglected. Introducing this effect in our calculations with ($\alpha_R = 2\times 10^{-11}$ (eV m)), we have presented in Fig. 7b the variation of Helmholtz free energy vs temperature for two confinement strength $\hbar\omega_0$ = 4.2 and $\hbar\omega_0$ = 16.9 meV for B = 20 T. As we can remark, the Helmholtz free energy is more important for high confinement strength. This behavior has already been encountered by several authors [28,60]. We also note that the effect of polaron is more important for strong confinement cases. The shift is about 0.6 eV for $\hbar\omega_0$ = 4.2 meV and 0.12 eV for $\hbar\omega_0$ = 16.9 meV.

Finally, in Fig. 7c we plot the variation of Helmholtz free energy vs temperature for three values of the magnetic field (B = 10, 20 and 40 T). As it is well known, the magnetic field acts as additive confinement leading to a shift of energy levels, thus the entropy of the system lowers, leading to an increase of Helmholtz free energy. Our calculations show that the effect of the phonon is more important with increasing magnetic field intensity.

As we have already indicated the GaN admit a large coupling constant than $InAs$, α_{LO}^{GaN} = 0.439 and α_{LO}^{InAs} = 0.055. In order to analyze the impact of the coupling with phonon on the magnetic susceptibility we compare in Fig. 8 this physical parameter for GaN and $InAs$. Thus in this figure, we draw the susceptibility of $InAs$ (red color) and GaN (black color) for both cases with (Fig. 8a) and without phonon interaction (Fig. 8b). We have taken parameters such that l_0 takes the same value for $InAs$ and GaN. As it can be seen in Fig. 8a the susceptibility presents a peak in both cases of GaN and $InAs$. These peaks are situated at ω_c/ω_0 = 0.25 ($B \approx$ 1 T) for $InAs$ and ω_c/ω_0 = 9 ($B \approx$ 60 T) for GaN. We also remark that the both materials change their character from diamagnetic ($\chi \prec 0$) to paramagnetic ($\chi \succ 0$) indicated by horizontal red line (black line) for $InAs$ (GaN). These

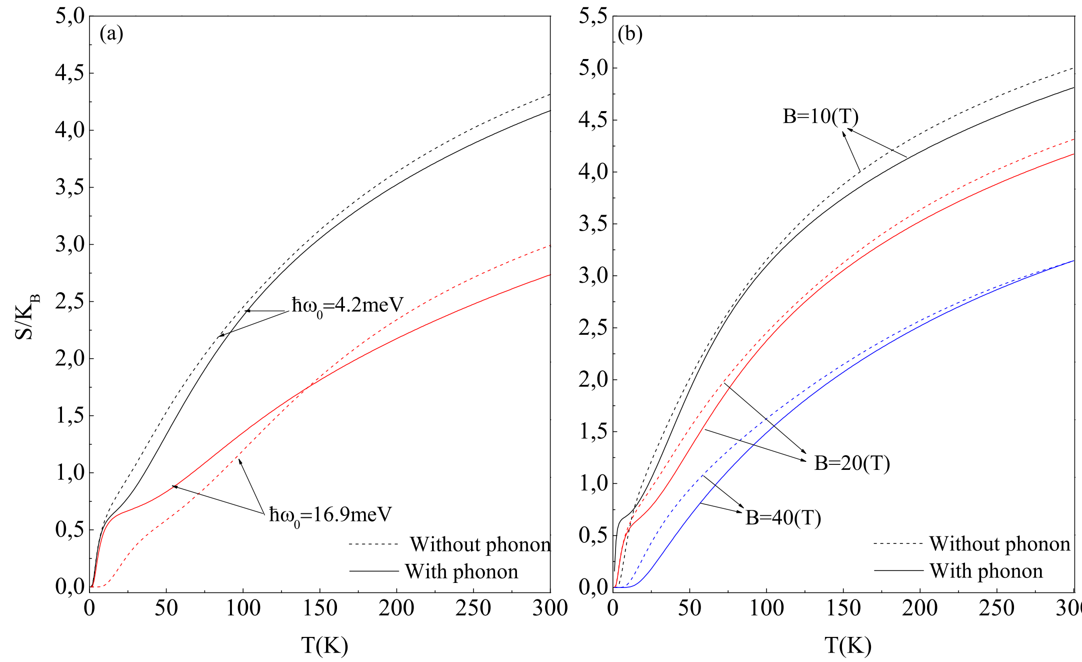

Fig. 6. Plot of entropy for GaN vs temperature, (a) for two values of confinement strength $\hbar\omega_0 = 4.2$ meV, *and* $\hbar\omega_0 = 16.9$ meV at $B = 20T$ and $\alpha_R = 2\times10^{-11}$ (eV m). (b) for three values of magnetic field strength $B = 10, B = 20$ and $B = 40$ T, with $\hbar\omega_0 = 4.2$ meV, and $\alpha_R = 2\times10^{-11}$ (eV m). The dashed lines and solid lines are associated without and with polaron effect, respectively in all figures.

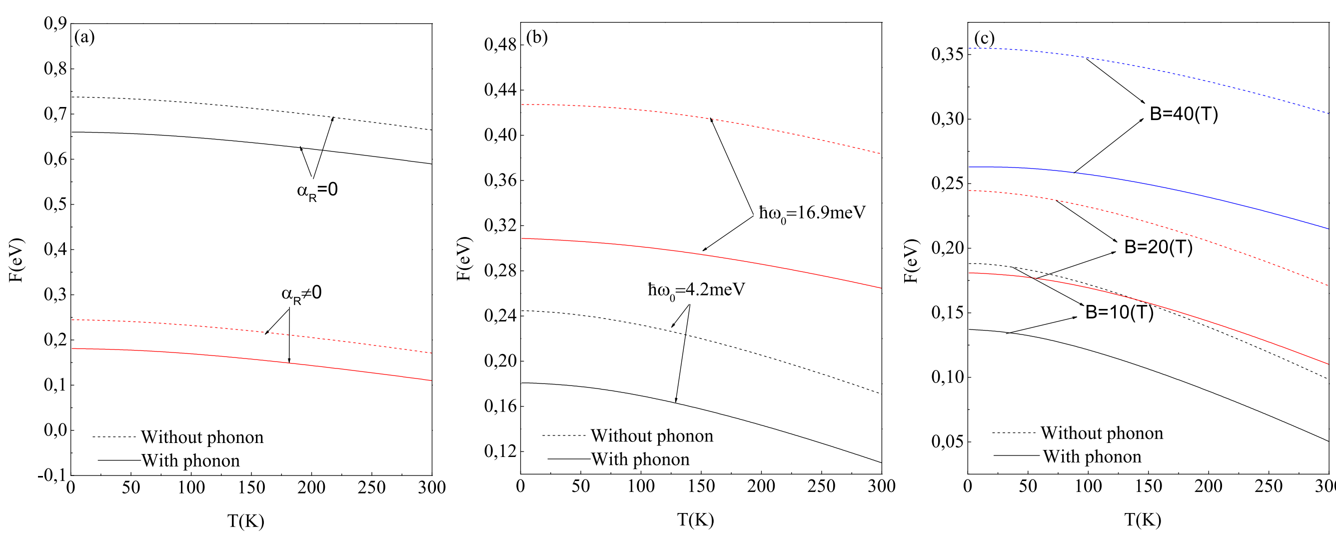

Fig. 7. Plot of Helmholtz free energy for GaN vs temperature (a) for two values of confinement strength $\hbar\omega_0 = 4.2$ meV, *and* $\hbar\omega_0 = 16.9$ meV at $B = 20$ T and $\alpha_R = 2\times10^{-11}$ (eV m). (b) for three values of magnetic field strength $B = 10, B = 20$ and $B = 40$ T, with $\hbar\omega_0 = 4.2$ meV, and $\alpha_R = 2\times10^{-11}$ (eV m). (c) without and with RSOI at $B = 20$ T and $\hbar\omega_0 = 4.2$ meV. The dashed lines and solid lines are associated without and with polaron effect, respectively in all figures.

changes of diamagnetic character held at $\omega_c/\omega_0 = 0.62$ ($B \approx 2.34$ T) for $InAs$ and $\omega_c/\omega_0 = 7$ ($B \approx 46$ T) for GaN. With further increase in the magnetic field, all curves drop and the materials change the characters and retrieve their diamagnetic behavior. Fig. 8b, we present the case where the e-phonon is taken into account. First, all the peaks are less pronounced with a right (left) shift for $InAs$ (GaN) i.e. to height (low) magnetic field. We also note that the system changes from diamagnetic to paramagnetic but reaches to saturation limit conserving a paramagnetic character.

4. Conclusions

In this work, we have presented a study of the effect of spin–orbit interaction and the interaction between *electron*-phonon on the magnetic and thermodynamic properties of 2-D quantum structures. Our results further demonstrate that the thermodynamic and magnetic properties depend strongly on the magnetic field, *electron*-phonon - interaction, and the Rashba SOI. It is well known that magnetic susceptibility is an important quantity that defines the magnetic nature of the material as diamagnetic or paramagnetic and also to study whether diamagnetic to paramagnetic conversion is possible in presence of the magnetic field, or if there are parameters that can control this transition. It is interesting to note that even at $B = 0T$, the susceptibility of GaN shows

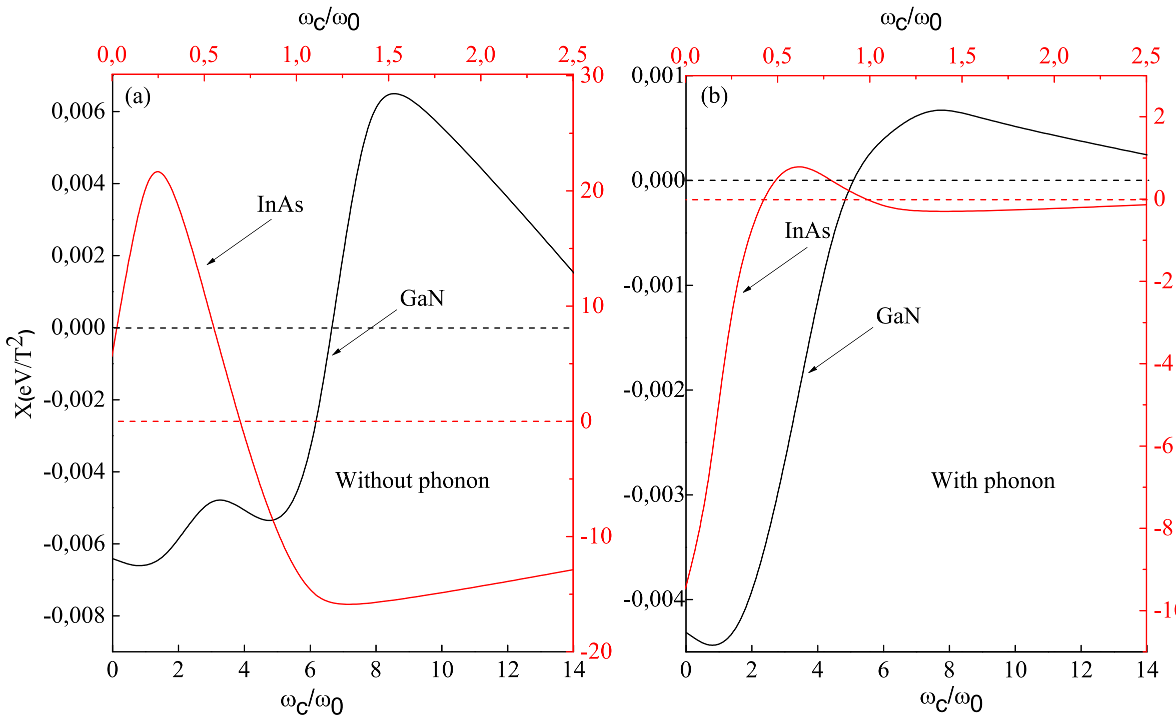

Fig. 8. Plot of susceptibility of GaN and InAs QD as function of ω_c/ω_0 (l_0 = 10 nm and $\hbar\omega_0$ = 4.2 meV). The dashed lines and solid lines are represent the case without and with RSOI respectively ($\alpha_R = 0$ (eV m) and $\alpha_R \neq 0$ (eV m)).

diamagnetic behavior for all temperatures, with an increase in the magnetic field, susceptibility increases and the system shows paramagnetic behavior for both cases associated with and without polaron effect. The susceptibility for $InAs$ increases with the magnetic field, reaches a maximum, and then again decreases to negative values and then takes a minimum value on further increasing magnetic field, it shows a dip and then increases slightly i.e. transition from paramagnetic to diamagnetic takes place. However, with the introduction of spin–orbit interaction, the cutoff magnetic field Bc(where the magnetic nature of the dot changes over from diamagnetic to paramagnetic) shifts to the higher magnetic field we observed that with an increase in temperature, the mean energy of the system also increases, also with an increase in confinement and magnetic field strength, the mean energy increases. The presence of the polaron effect RSOI lowers the mean energy of the system. The heat capacity curve shows a peak at a low temperature (Schottky anomaly) and a shift toward high temperature with an increase in confinement and magnetic field strength. The consideration of the polaron effect shifts the heat capacity curve to lower temperatures. The entropy of the system increases with an increase in temperature as it increases the randomness of the system by increasing the energy. With a decrease in confinement and magnetic field strength the entropy increases. The polaron effect consideration increases the entropy.

CRediT authorship contribution statement

K. Lakaal: Analytical and numerical Investigations, Data curation. **M. Kria:** Numerical validation, Software, Validation. **J. El Hamdaoui:** Numerical validation, Software, Validation. **Varsha:** Formal anaysis, Investigation, Contribution in the analysis of the results, Writing – review & editing. **V. Prasad:** Idea, Conceptualization, Writing – original draft, Writing – review & editing. **Vijit V. Nautiyal:** Formal anaysis, Investigation, Contribution in the analysis of the results. **M. El-Yadri:** Data curation, Software. **L.M. Pérez:** Contribution in the analytical part, Visualization, Software, Participation in the discussions of results, Writing – review & editing. **D. Laroze:** Contribution in the analytical part, Funding acquisition, Visualization, Software, Participation in the discussions of results. **E. Feddi:** Idea, Conceptualization, Writing – original draft, Writing – review & editing, All authors have read and agreed to the published version of the manuscript.

Declaration of competing interest

The authors declare that they have no known competing financial interests or personal relationships that could have appeared to influence the work reported in this paper.

Acknowledgments

LMP acknowledges financial support from ANID, Chile through Convocatoria Nacional Subvención a Instalación en la Academia Convocatoria Año 2021, Grant SA77210040. LMP and DL acknowledge partial financial support from FONDECYT, Chile 1180905. DL acknowledges partial financial support from Centers of excellence with BASAL/ANID, Chile financing, AFB180001, CEDENNA.

References

[1] T. Shinjo, Nanomagnetism and Spintronics, Elsevier Science, 2009.
[2] C. Gong, X. Zhang, Science 363 (2019) 6428.
[3] T. Gunst, T. Markussen, K. Stokbro, M. Brandbyge, Phys. Rev. B 93 (3) (2016) 035414.
[4] S. Maekawa, Concepts in Spin Electronics, Oxford Univ Press, 2006.
[5] B. Divinskiy, S. Urazhdin, S.O. Demokritov, V.E. Demidov, Nature Commun. 10 (1) (2019) 1.
[6] L. Wenqing, X. Yongbing, Spintronic 2D Materials: Fundamentals and Applications, Elsevier, 2019.
[7] G. Dresselhaus, Phys. Rev. 100 (2) (1955) 580.
[8] E.I. Rashba, Soviet Phys. Solid State 2 (1960) 1109.
[9] B. Gisi, S. Sakiroglu, Kasapoglu, H. Sari, I. Sokmen, Superlattices Microstruct. 86 (2015) 166.
[10] B. Vaseghi, A. Ghaffari, Physica E 81 (2016) 163.
[11] V.V. Nautiyal, P. Silotia, Phys. Lett. A 382 (2018) 2061.
[12] V. Nautiyal, D. Munjal, P. Silotia, J. Magn. Magn. Mater. 528 (2021) 167688.
[13] R. Rani, V. Kumar, R.M. Singh, F. Chand, Ind. J. Phys. 94 (2020) 1705.
[14] S.E. Pourmand, G. Rezaei, B. Vaseghi, Eur. Phys. J. B 92 (2019) 1.
[15] V.A. Dalkhani, S.G. Nobandegani, M.J. Karimi, Eur. Phys. J. B 92 (2019) 19.

[16] A. Ghafari, B. Vaseghi, G. Rezaei, S.F. Taghizadeh, M.J. Karimi, Superlattices Microstruct. 101 (2017) 397.
[17] B. Vaseghi, V. Azizi, M. Khosran, Z. Owjifard, Eur. Phys. J. D. 73 (2019) 51.
[18] B. Vaseghi, G. Rezaei, M. Malian, Opt. Commun 287 (2013) 241.
[19] P. Hosseinpour, J. Barvestani, A. Soltani-Vala, Phys. Scr. 91 (4) (2016) 045803.
[20] Y. Khoshbakht, R. Khordad, H.R. Rastegar Sedehi, J. Low Temp. Phys. 202 (2021) 59.
[21] U. Meirav, M.A. Kastner, S.J. Wind, Phys. Rev. Lett. 65 (6) (1990) 771.
[22] R.C. Ashoori, H.L. Stormer, J.S. Weiner, L.N. Pfeifer, K.W. Baldwin, K.W. West, Phys. Rev. Lett. 71 (1993) 613.
[23] H. Drexler, D. Leonard, W. Hansen, J.P. Kotthaus, P.M. Petroff, Phys. Rev. Lett. 73 (16) (1994) 2252.
[24] S. Tarucha, D.G. Austing, T. Honda, R.J. van der Hage, L.P. Kouwenhoven, Phys. Rev. Lett. 77 (17) (1996) 3613.
[25] B. Szafran, J. Adamowski, S. Bednarek, Physica E 4 (1) (1999) 1.
[26] M. Wagner, U. Merkt, A.V. Chaplik, Phys. Rev. B 45 (4) (1992) 1951.
[27] S. Bednarek, B. Szafran, J. Adamowski, Phys. Rev. B 59 (20) (1999) 13036.
[28] M.Z. Malik, D.S. Kumar, S. Mukhopadhyay, A. Chatterjee, Physica E 121 (2020) 114097.
[29] J.L. Zhu, Z.Q. Li, J.Z. Yu, K. Ohno, Y. Kawazoe, Phys. Rev. B 55 (1997) 15819.
[30] A. John Peter, S. Saravana Kumar, Physica E 41 (2008) 138.
[31] A. Rejo Jeice, K. Navaneethakrishnan, Braz. J. Phys. 39 (2009) 526.
[32] N.G. Aghekyan, E.M. Kazaryan, A.A. Kostanyan, H.A. Sarkisyan, Superlattices Microstruct. 50 (2011) 199.
[33] T. Prosted, J.P. Hansen, C.J. Wesslen, E. Lindroth, E. Rsnen, Eur. Phys. J. B 86 (2013) 430.
[34] E. Sadeghi, M. Moradi Lm, Physica E 70 (2015) 141.
[35] A. Boda, D.S. Kumar, I.V. Sankar, A. Chatterjee, J. Magn. Magn. Mater. 418 (2016) 242.
[36] M. Taut, Phys. Rev. A 48 (5) (1993) 3561.
[37] D.S. Kumar, S. Mukhopadhyay, A. Chatterjee, J. Magn. Magn. Mater. 418 (2016) 169–174.
[38] R. Khordad, J. Magn. Magn. Mater 449 (2018) 510.
[39] R. Khordad, B. Vaseghi, Int. J. Quant. Chem. 119 (20) (2019) e25994.
[40] S. Nakamura, M. Senoh, S. Nagahama, N. Iwasa, T. Yamada, T. Matsushita, H. Kiyoku, Y. Sugimoto, Japan. J. Appl. Phys. 35 (1996) L217.
[41] K.E. Bakkari, A. Sali, E. Iqraoun, A. Ezzarfi, Superlattices Microstruct. 148 (2020) 106729.
[42] Y.F. Huangfu, Z.W. Yan, Phys. E 40 (2008) 2982.
[43] D.V. Melnikov, W.B. Fowler, Phys. Rev. B 64 (2001) 195335.
[44] A. Nazir, D.P.S. McCutcheon, J. Phys.: Condens. Matter 28 (2016) 103002.
[45] E. Feddi, M. El Haouari, E. Assaid, B. Stébé, J. El Khamkhami, F. Dujardin, Phys. Rev. B 68 (23) (2003) 235313.
[46] J. El Khamkhami, E. Feddi, E. Assaid, F. Dujardin, B. Stébé, M. El Haouari, Phys. E 25 (4) (2005) 366.
[47] M. El Haouari, E. Feddi, F. Dujardin, R.L. Restrepo, M.E. Mora-Ramos, C.A. Duque, Superlattices Microstruct. 111 (2017) 457.
[48] T.D. Lee, F.E. Low, D. Pines, Phys. Rev. 90 (2) (1953) 297.
[49] S.I. Pekar, Research on Electron Theory of Crystals, AEC, Division of Technical Information, Washington, D. C, 1963;
S.I. Pekar, Untersuchungen uber die Elektronentheorie der Kristalle, Akademie-Verlag, Berlin, 1954.
[50] M. Germain, E. Kartheuser, A.L. Gurskii, E.V. Lutsenko, I.P. Marko, V.N. Pavlovskii, B. Schineller, J. Appl. Phys. 91 (12) (2002) 9827.
[51] M. Ziesmann, D. Heitmann, L.L. Chang, Phys. Rev. B 35 (9) (1987) 4541.
[52] M.E. Levinshtein, S.L. Rumyantsev, M.S. Shur, John Wiley and Sons, New York, 2001.
[53] B. Santic, Semicond. Sci. Technol. 18 (2003) 219.
[54] L. Xi-Xia, B. Shi-Liang, Chin. Phys. 13 (1) (2004) 71.
[55] M. Solaimani, L. Lavaei, S.M.A. Aleomraninejad, J. Opt. Soc. Amer. B 34 (9) (2017) 1989–1993.
[56] S. Baskoutas, A.F. Terzis, W. Schommers, J. Comp. Theor. Nanosc. 3 (2006) 269.
[57] P. Hosseinpour, J. Barvestani, A.S. Vala, Phys. Scr. 91 (2016) 045803.
[58] O. Voskoboynikov, O. Bauga, C.P. Lee, O. Tretyak, J. Appl. Phys. 94 (9) (2003) 5891–5895.
[59] K. Feddi, M. Kria, M. El-Yadri, F.F. Mbognou, G. Long, A. Tiutiunnyk, E. Feddi, Phys. Scr. 95 (10) (2020) 105706.
[60] M. Kria, K. Feddi, N. Aghoutane, M. El-Yadri, L.M. Pérez, D. Laroze, E. Feddi, Physica A 560 (2020) 125104.